Resonance-induced synchronization in coupled phase oscillators with bimodal frequency distribution and periodic coupling

Sansan Li[1] and Xingang Wang[2,*]

[1]*School of Mathematics and Information Science, North Minzu University, Yinchuan 750021, China*
[2]*School of Physics and Information Technology, Shaanxi Normal University, Xi'an 710062, China*

Synchronization behaviors in globally coupled phase oscillators with symmetric bimodal frequency distribution and periodic coupling are studied. It is found that by a proper setting of the frequency of the periodic coupling, the synchronization propensity of the oscillators can be markedly improved. Specifically, we show that when the frequency of the periodic coupling matches the distance of the central frequencies in the distribution, the critical coupling characterizing the onset of synchronization can be substantially decreased. The mechanism behind the phenomenon of periodic-coupling-enhanced synchronization is analyzed by the methods of Ott-Antonsen ansatz and synchronization transition tree, and it is revealed that the synchronization enhancement is attributed to the resonance between the synchronization clusters and the periodic coupling.

I. INTRODUCTION

The Kuramoto model serves as a simple paradigm for exploring the synchronization phenomena observed ubiquitously in nature and human-made systems [1–3]. Coined in 1975, the classic Kuramoto model consists of an ensemble of globally coupled phase oscillators, with the natural frequencies of the oscillators following an unimodal symmetric distribution [4]. In studying the synchronization behaviors in the Kuramoto model, one of the central tasks is to find the critical point where the synchronization is started, namely the critical coupling strength where the synchronization order parameter begins to increase from zero [4,5]. By the approach of mean-field coupling, Kuramoto gave an analytical prediction for the critical coupling, as well as the behavior of the synchronization order parameter in the vicinity of the onset point. Over the past half-century, the Kuramoto model and its generalized forms have been extensively studied by researchers from different fields, in which plenty of new dynamical phenomena have been reported and the underlying mechanisms have been unveiled [2,3]. In particular, stimulated by the blooming of network science, considerable attention has been paid to the synchronization behaviors in complex network systems in recent years, where the important roles of network structures on synchronization have been uncovered [6,7].

Besides the onset point for synchronization, attention has been also paid to the transition path from desynchronization to global synchronization in Kuromoto-like models [8–12]. In exploring synchronization transition, one of the key issues is to characterize the partial synchronization behaviors generated at different coupling strengths [2,3]. Roughly, partial synchronization refers to the coherent motion of a fraction of the oscillators, which is typically observed at intermediate couplings [13–16]. In partial synchronization, the phase oscillators are self-organized into different groups (clusters), with the effective frequencies of the oscillators inside each group approximately the same but are of clear difference for oscillators from different groups.

The organization of the partial synchronization states can be affected by several factors. For the classic Kuramoto model, the grouping of the oscillators is determined solely by their natural frequencies [15]; for lattice networks, the grouping is also influenced by the spatial distances of the oscillators [17]; for complex networks, the network topology plays an important role in forming the clusters [9]. Additionally, the organization of the synchronization clusters is dependent on the coupling strength. For the classic Kuromoto model, as the coupling strength increases from the onset point, first a small-size synchronization cluster will appear (by oscillators whose natural frequencies are close to the mean frequency), then the cluster will expand gradually by recruiting more oscillators and, once all oscillators are synchronized in phase, the system reaches the global synchronization state [8–11].

Along with the growth of the clusters, the synchronization order parameter will be increased gradually from zero (at the onset point) to unity (for the global synchronization state), presenting a second-order phase transition. This picture of synchronization transition, however, is dramatically changed when the natural frequencies of the oscillators are not of unimodal distribution [18–23], or when the oscillators are coupled on complex networks [7–11]. For instance, when the oscillators are coupled through a scale-free complex network in such a way that their natural frequencies are positively correlated with their degrees, the synchronization order parameter might suddenly increase from zero to a large value as the coupling strength exceeds a critical threshold, showing the phenomenon of "explosive synchronization" [11].

From the perspective of network control, a question of broad interest is how the synchronization behaviors of

---

*Contact author: wangxg@snnu.edu.cn

coupled oscillators can be manipulated by external drivings. For biological and neural systems, an issue of particular concern is how the synchronization behaviors respond to the externally added periodic signals, e.g., the effects of seasonal variations on ecological processes [24], the influences of circadian rhythm on neural activities [25], the impacts of diurnal cycles on gene expressions [26], and the influences of electrical and magnetic stimulations on the electrophysiological activities of human brain [27]. In particular, with the development of modern techniques in medicine and neuroscience (e.g., transcranial electrical and magnetic stimulations), in recent years tremendous efforts have been paid to the treatment of neurological disorders, or the improvement of brain cognitive functions, by noninvasive electrical and magnetic simulations [28,29]. In these applications, an urgent issue is to evaluate the efficacy of the external stimulations in manipulating the collective neuronal behaviors.

Typically, external drivings participate in the system dynamics through two approaches: acting on the oscillator states or influencing the oscillator couplings. For the former, the driving signals can be regarded as released from an external phase oscillator, and the system responses can be analyzed under the framework of synchronization (the external oscillator is coupled to the internal oscillators in a one-way fashion) [30–33]. The latter, however, might give rise to very complicated dynamics whose analysis requires sophisticated techniques. For instance, it is demonstrated that when the coupling strength between chaotic oscillators changes periodically with time, the synchronization propensity of the oscillators can be significantly improved by a proper setting of the frequency of the periodic coupling [34–36]. Similar studies have been also conducted for the classic Kuramoto model recently, where it is observed that, in contrast to the results of chaotic oscillators, the adoption of period coupling suppresses synchronization in general. Specifically, it is shown that with the decrease of the driving frequency of the periodic coupling, the synchronization performance is gradually deteriorated [37]. Given the important implications of the Kuramoto model to the functionality of a wide range of real-world systems, it is natural to ask the following questions: *Can periodic coupling enhance synchronization in the Kuramoto model? And, if yes, when and why?*

Intrigued by the above questions, we investigate in the present work the synchronization behaviors of coupled phase oscillators under timely periodic couplings, with the natural frequencies of the oscillators following a bimodal distribution. Our main findings are as follows: (1) the synchronization performance of the system can be markedly improved by a proper setting of the frequency of the periodic coupling, with the optimal frequency determined by the central frequencies of the bimodal distribution; and (2) under the optimal driving frequency, the synchronization order parameter is not increased monotonically with the coupling strength, but showing a crossover in the transition to global synchronization. By the methods of dimension reduction and synchronization transition trees, we conduct an analysis on the mechanism underlying the observed phenomena. It is found that both phenomena are induced by the resonance between the synchronization clusters and the periodic driving. To be specific, the improved synchronization performance is due to the

resonance between the synchronization clusters and the periodic driving under weak couplings, and the crossover of the synchronization order parameter is due to the newly generated synchronization clusters induced by the periodic driving under strong couplings. The findings shed light onto the collective behaviors of coupled oscillators in response to external drivings and provide an alternative approach for manipulating the synchronization behaviors in complex dynamical systems.

II. MODEL AND PHENOMENA

A. Model

Our model of coupled phase oscillators reads

$$\dot{\theta}_i = \omega_i + \frac{K(t)}{N} \sum_{j=1}^{N} \sin(\theta_j - \theta_i), \tag{1}$$

where $i, j = 1, \ldots, N$ are the oscillator indices, N is the system size, and $\theta_i(t)$ is the instant phase of the ith oscillator. ω_i is the natural frequency of the ith oscillator, which follows the distribution $g(\omega)$. $K(t)$ represents the time-dependent coupling strength.

Different from the classic Kuramoto model in which the coupling strength is a constant and the natural frequency follows an unimodal distribution, here we adopt the scheme of periodic coupling, $K(t)$, and choose the natural frequencies from the bimodal Lorentzian (Cauchy) distribution. Specifically, we set in Eq. (1)

$$K(t) = K_0[1 + \sin(\Omega t)], \tag{2}$$

and

$$g(\omega) = \frac{\Delta}{2\pi} \left[\frac{1}{(\omega - \omega_0)^2 + \Delta^2} + \frac{1}{(\omega + \omega_0)^2 + \Delta^2} \right]. \tag{3}$$

In Eq. (2), Ω and K_0 denote, respectively, the frequency and amplitude of the periodic coupling. We note that the cost of the periodic coupling (i.e., the time-averaged coupling) is kept unchanged when varying Ω, i.e., $\langle K(t) \rangle = K_0$. Our main objective in the present work is to demonstrate and argue that under the same coupling cost, the synchronization performance can be improved by a proper setting of Ω. In Eq. (3), $\pm \omega_0$ are the central frequencies of the Lorentzian distribution (i.e., the locations of the distribution peaks), and Δ characterizes the half-width of the peaks. The distance between the central frequencies therefore is $2\omega_0$. Without the loss of generality, we set $\Delta = 1$ and choose $g(\omega)$ to be symmetric about $\omega = 0$. [If $g(\omega)$ is symmetric about the frequency $\tilde{\omega} \neq 0$, we can analyze the synchronization behavior of the phase oscillators in the rotating frame by replacing $\theta_i(t)$ with $\theta_i(t) - \tilde{\omega} t$ [3,38]. In the rotating frame, the system dynamics is still governed by Eq. (1), with the frequency distribution identical to Eq. (3).] To make the distribution bimodal, we keep $\omega_0 > \Delta/\sqrt{3}$ in the current study (the distribution will be unimodal if this condition is not satisfied). In numerical simulations, the system size is fixed as $N = 2 \times 10^4$. The initial phases of the oscillators are randomly chosen within the range $(0, 2\pi)$, and Eq. (1) is evolved numerically by the fourth-order Runge–Kutta algorithm with the time step $\delta t = 1 \times 10^{-2}$.
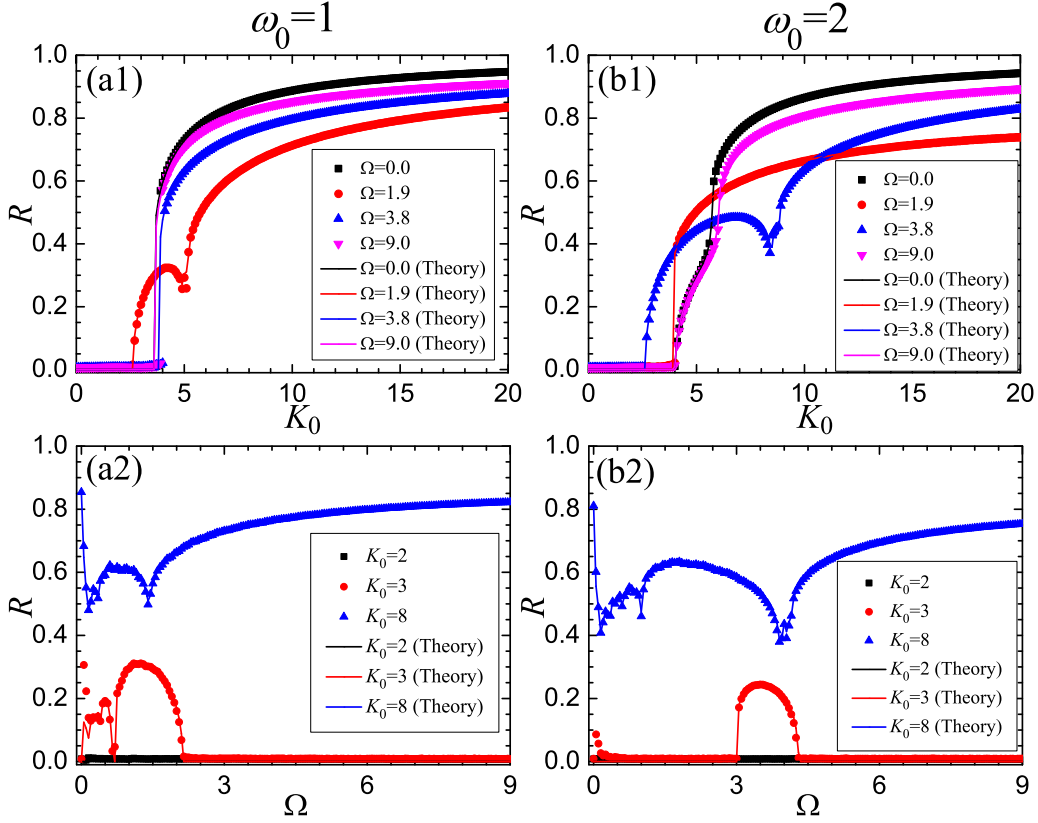
FIG. 1. The impacts of periodic coupling on the synchronization performance of $N = 2 \times 10^4$ globally coupled phase oscillators. (a1) For $\omega_0 = 1.0$, the variation of the synchronization order parameter, R, with respect to the coupling amplitude, K_0, under different driving frequencies, Ω. The critical coupling is about $K_c = 2.6$ for $\Omega = 1.9$, and is about $K_c = 3.6$ for the other driving frequencies. (a2) For $\omega_0 = 1.0$, R versus Ω under different coupling amplitudes, K_0. The optimal frequency for $K_0 = 3$ is $\Omega_o \approx 1.5$. [(b1) and (b2)] Results for $\omega_0 = 2.0$. For $\Omega = 3.8$, the critical coupling in (b1) is about $K_c = 2.7$. The optimal driving frequency for $K_0 = 3$ in (b2) is about $\Omega_o \approx 3.9$. Colored symbols represent the numerical results. Colored lines represent the theoretical predictions of the reduced model.

Following Ref. [4], we characterize the synchronization performance by the order parameter

$$R = \langle R(t) \rangle_T = \left\langle \frac{1}{N} \left| \sum_{j=1}^{N} e^{\mathbf{i}\theta_j} \right| \right\rangle_T, \qquad (4)$$

where $\mathbf{i} = \sqrt{-1}$ is the imaginary unit, $| \cdot |$ represents the modulus function, and $\langle \cdot \rangle$ denotes that the result is averaged over time period T. In calculating R, the system is first evolved for a transient period $T' = 200$, and then the result is averaged over a period $T = 100$. We have $R \in [0, 1]$, with $R = 0$ and 1 corresponding to the complete desynchronization and global synchronization states, respectively.

B. Numerical results

We start by investigating the impacts of the periodic coupling on the synchronization performance. Setting $\omega_0 = 1$ in the frequency distribution, we plot in Fig. 1(a1) the variation of R with respect to K_0 (the amplitude of the periodic coupling) for different values of Ω (the frequency of the periodic coupling). The benchmark results obtained for the constant coupling ($\Omega = 0$) are plotted in the figure as the comparison (the blacked squares), which shows that the onset of synchronization occurs at about $K_c = 3.6$ and, as K_0 increases

from K_c, the value of R is suddenly increased to a large value ($\sim$0.5) and then is increased monotonically, showing a first-order phase transition. (The first-order phase transition is typically observed in Kuramoto-like models with the natural frequencies of the oscillators following a bimodal distribution, and the underlying mechanism is normally attributed to the formation and competition of the synchronization clusters [18–23].) Changing Ω to 3.8 (the blue up-triangles), we see that the critical coupling K_c is almost unchanged, but in the transition regime ($K_0 > K_c$) the synchronization order parameter is clearly below that of constant coupling. Similar results are also observed for the driving frequency $\Omega = 9.0$ (the pink down-triangles). Compared to the results of $\Omega = 3.8$, we see that the synchronization performance of $\Omega = 9.0$ is improved but is still below the benchmark results of constant coupling. These results are consistent with the findings in Ref. [37], where it is shown that periodic coupling deteriorates synchronization in general, and the slower the driving frequency, the smaller the synchronization order parameter in the transition regime. However, abnormal synchronization phenomena are observed for $\Omega = 1.9$ (the red dots). The anomalies are manifested in two aspects. First, the critical coupling K_c is notably decreased. Specifically, the critical coupling is decreased to $K_c \approx 2.6$ for the driving frequency $\Omega = 1.9$. Second, in the transition regime, the value of R is not increased

monotonically with K_0. To be specific, a crossover is observed in the variation of R around $K_0 = 5$. Numerical evidence in Fig. 1(a1) thus suggests that for the bimodal Lorentzian distribution described by Eq. (3), the adoption of periodic coupling indeed can improve the synchronization performance if the driving frequency is set properly.

Is there an optimal driving frequency by which the synchronization performance is maximized, and does the phenomenon of periodic-coupling-enhanced synchronization depend on the coupling amplitude K_0? To address these questions, we next check the variation of R with respect to Ω for different values of K_0 based on simulations. As the demonstration, we choose the coupling amplitudes as $K_0 = (2, 3, 8)$. The numerical results are presented in Fig. 1(a2). We see that for $K_0 = 2$ (the black squares), the value of R is staying always at 0, indicating that the synchronization performance is not affected by periodic coupling in the case of weak couplings. However, the results for $K_0 = 3$ show that the synchronization performance is significantly affected by tunning the driving frequency (the red dots). Specifically, we see in the figure that R reaches its maximum at the frequency $\Omega_o \approx 1.5$. The variation of R shows new features when $K_0 = 8$ (the blue up-triangles). In this case, the adoption of periodic coupling always deteriorates the synchronization performance ($R \approx 0.85$ when $\Omega = 0$) and, interestingly, around the optimal frequency Ω_o the synchronization performance is the worst. The results in Fig. 1(a2) confirm the existence of an optimal frequency in improving synchronization but also point out that the influence of periodic coupling on synchronization is dependent on the coupling amplitude, i.e., the synchronization performance is improved only for the intermediate coupling amplitudes.

To check the generality of the above phenomena, we set $\omega_0 = 2$ and plot in Fig. 1(b) the variation of R with respect to K_0 and Ω. We see in Fig. 1(b1) that the critical coupling K_c characterizing the onset of synchronization is decreased when the coupling frequency is $\Omega = 3.8$. Still, it is observed that in the transition regime, the value of R is first increased and then decreased, with the crossover appearing at about $K_0 = 8.4$. Figure 1(b2) shows again that the impact of periodic coupling on synchronization is dependent on the coupling amplitude. For the intermediate coupling amplitude $K_0 = 3$, the optimal frequency is changed to $\Omega_o \approx 3.9$. The results for $\omega_0 = 2$ shown in Fig. 1(b), while confirming the modulating effects of periodic coupling on synchronization, show also that the synchronization performance is dependent on the properties of the frequency distribution (i.e., the parameter ω_0).

The new phenomena we have observed in simulations can be summarized as follows. First, periodic coupling can improve synchronization, but only under the intermediate coupling amplitudes. Second, when synchronization is improved by the periodic coupling, the synchronization order parameter shows a crossover in the transition regime. Third, the optimal frequency for synchronization is dependent on the frequency distribution of the oscillators, i.e., the central frequencies $\pm \omega_0$. An exploration of the mechanism underlying the observed phenomena is our mission in the next section.

III. MECHANISM ANALYSIS

The mechanism of periodic-coupling-enhanced synchronization is analyzed through two approaches: dimension reduction and synchronization transition tree. The former focuses on the macroscopic behaviors of the oscillators, which will be employed to unveil the improving effect of periodic coupling on synchronization. The latter focuses on the microscopic behaviors of the oscillators, which will be utilized to interpret the crossover of the synchronization order parameter in the transition regime.

A. The approach of dimension reduction

We adopt the method of Ott-Antonsen (OA) ansatz to reduce the dimension of the system dynamics [39]. This method has been adopted widely in the literature for exploring the collective dynamics of coupled phase oscillators, which is able to not only predict the onset point for synchronization, but also estimate the synchronization order parameter in the transition regime (see Ref. [38] and references therein for more details). In what follows, we first generalize the OA method to oscillators with bimodal frequency distribution and then utilize the generalized method to explore the enhancing mechanism of periodic coupling on synchronization.

Let $N \to \infty$ in Eq. (1), the probability density function $p(\theta, \omega, t)$ follows the continuity equation

$$\frac{\partial p(\theta, \omega, t)}{\partial t} + \frac{\partial [\upsilon_\theta p(\theta, \omega, t)]}{\partial \theta} = 0, \quad (5)$$

with

$$\upsilon_\theta(\theta, \omega, t) = \omega + \frac{K(t)}{2\mathbf{i}}[z(t)e^{-\mathbf{i}\theta} - z^*(t)e^{\mathbf{i}\theta}], \quad (6)$$

and

$$z(t) = R(t)e^{\mathbf{i}\phi} = \int_0^{2\pi} d\theta \int_{-\infty}^{+\infty} p(\theta, \omega, t)e^{\mathbf{i}\theta} d\omega. \quad (7)$$

Here $z^*(t)$ denotes the complex conjugate of $z(t)$, and ϕ represents the phase associated with the order parameter R. Expanding $p(\theta, \omega, t)$ with respect to θ by the Fourier series, we have

$$p(\theta, \omega, t) = \frac{g(\omega)}{2\pi}\left[1 + \sum_{n=1}^{\infty} p_n(\omega, t)e^{-\mathbf{i}n\theta} + \sum_{n=1}^{\infty} p_n^*(\omega, t)e^{\mathbf{i}n\theta}\right]. \quad (8)$$

Using the Ott-Antonsen ansatz [39]

$$p_n(\omega, t) = [a(\omega, t)]^n, |a(\omega, t)| \leqslant 1,$$

and plugging Eq. (8) into Eqs. (5) and (7), we have

$$\frac{\partial a}{\partial t} + \mathbf{i}\omega a + \frac{K(t)}{2}[z(t)a^2 - z^*(t)] = 0, \quad (9)$$

and

$$z^*(t) = \int_{-\infty}^{\infty} a(\omega, t)g(\omega)d\omega. \quad (10)$$

For the bimodal Lorentzian distribution described by Eq. (3), there are two poles in the lower ω-complex plane, $\omega = \pm\omega_0 - \mathbf{i}\Delta$. As such, the integration of Eq. (10) gives $z(t) = [z_1(t) + z_2(t)]/2$, with $z_{1,2}(t) = a^*(\pm\omega_0 - \mathbf{i}\Delta, t)$ representing, respectively, the synchronization order parameters of the two clusters formed by oscillators whose natural frequencies are close to ω_0 and $-\omega_0$ [18–23]. Combining Eqs. (9) and (10), we have the following equations for the time evolution of $z_1(t)$ and $z_2(t)$:

$$\dot{z}_1 = -(\Delta + \mathbf{i}\omega_0)z_1 + K(t)\big[z_1 + z_2 - (z_1^* + z_2^*)z_1^2\big]/4,$$

$$\dot{z}_2 = -(\Delta - \mathbf{i}\omega_0)z_2 + K(t)\big[z_1 + z_2 - (z_1^* + z_2^*)z_2^2\big]/4. \quad (11)$$

Due to the symmetric distribution of the natural frequencies, we have $|z_2| = |z_1| = \rho$ and $z_2/z_1 = e^{\mathbf{i}\psi}$, with ρ the synchronization order parameter of the synchronization clusters and ψ the phase difference between the two clusters. (Please see Appendix for the mathematical proof and Ref. [40] for the numerical verifications.) With this property, Eq. (11) can be rewritten as

$$\dot{\rho} = -\Delta\rho + K(t)\rho(1 - \rho^2)(1 + \cos\psi)/4,$$

$$\dot{\psi} = 2\omega_0 - K(t)(1 + \rho^2)\sin\psi/2. \quad (12)$$

Compared with the high-dimensional system described by Eq. (1), we see that the system dynamics is reduced to two coupled ordinary differential equations, which facilitates our analysis of the synchronization mechanism under periodic couplings. Now, to evaluate the synchronization performance, we only need to find the values of ρ and ψ by solving Eq. (12), and the synchronization order parameter is expressed as $R = \rho\sqrt{(1 + \cos\psi)/2}$. It is worth mentioning that different from the existing studies in which bimodal frequency distribution is adopted [18–23], here $K(t)$ is varying periodically with time [see Eq. (2) for the details]. To check the accuracy of the reduced model, we solve Eq. (12) numerically and plot in Fig. 1 the variations of R with respect to K_0 and Ω. We see that the results obtained from the reduced model are in good agreement with the results obtained from direct simulations in all the cases we have investigated.

Having justified the accuracy of the reduced model in characterizing the synchronization performance of the original system, we next employ this model to explore the synchronization mechanism under periodic couplings. For the sake of simplicity, here we consider the special case of on-off coupling, $K(t) = K_0 + K_0\,\mathrm{sgn}[\sin(\Omega t)]$, with $\mathrm{sgn}[\ldots]$ the sign function [34,35,37]. That is, the coupling strength is switching between 0 and $2K_0$ periodically with the time interval $2\pi/\Omega$. (Despite the simplification, on-off coupling captures the main features of the interaction between the synchronization dynamics and the periodic coupling. Please see the Supplemental Material for more details [40].) As $\rho = 0$ for the "off" intervals ($K = 0$), the synchronization order parameter is determined by the "on" intervals ($K = 2K_0$) under on-off coupling. Further, noticing that Eq. (12) cannot be solved analytically, we focus on only the steady states of the "on" intervals in exploring the synchronization mechanism. Setting $\dot{\rho} = \dot{\psi} = 0$ in Eq. (12), we obtain in total three steady states: $\rho = 0$ (the complete desynchronization state), $\mathcal{S}_1 = (\rho_1, \psi_1)$ and $\mathcal{S}_2 = (\rho_2, \psi_2)$ (the two partial synchronization states).
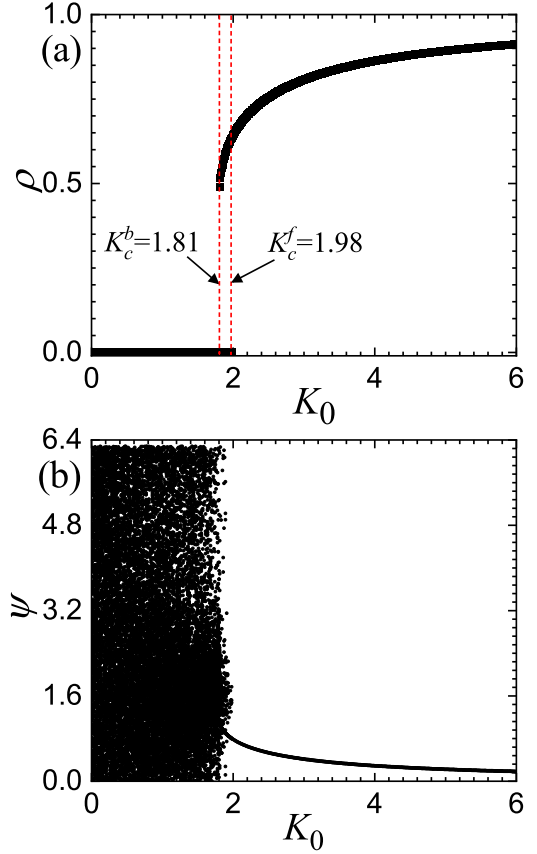

FIG. 2. The bifurcation diagram obtained from the reduced model. The results are obtained by solving Eq. (12) numerically with $K(t) = 2K_0$ and $\omega_0 = \Delta = 1$. (a) ρ versus K_0. The two critical couplings are $K_c^b \approx 1.81$ and $K_c^f \approx 1.98$. (b) ψ versus K_0. ψ is locked to constant values when $K_0 > K_c^f$, and is decreasing gradually as K_0 increases from K_c^f.

It is straightforward to find that the desynchronization state becomes unstable when $K_0 > K_c^f = 2\Delta$. The synchronization order parameter, ρ_1, of the steady state $\mathcal{S}_1$ is determined by the equation

$$-\Delta + \frac{K_0}{2}\big(1 - \rho_1^2\big)\left[1 + \sqrt{1 - \frac{4\omega_0^2}{K_0^2\big(1 + \rho_1^2\big)^2}}\right] = 0,$$

which has a solution when $K_0 > K_c^b = 2\Delta/(1 + \cos\psi_1)$, with $\psi_1 = \arcsin[2\omega_0/(K_0(1 + \rho_1^2))]$. Linear stability analysis shows that once it appears, the steady state $\mathcal{S}_1$ will be always locally stable. The synchronization order parameter, ρ_2, of the steady state $\mathcal{S}_2$ is determined by the equation

$$-\Delta + \frac{K_0}{2}\big(1 - \rho_2^2\big)\left[1 - \sqrt{1 - \frac{4\omega_0^2}{K_0^2\big(1 + \rho_2^2\big)^2}}\right] = 0,$$

which has no solution for $\rho \leqslant 1$ and therefore should be discarded. Theoretical analysis thus suggests that $\rho = 0$ for $K_0 < K_c^f$ and $\rho = \rho_1$ for $K_0 > K_c^b$. As $K_c^f > K_c^b$, the desynchronization state ($\rho = 0$) and the partial synchronization state $\mathcal{S}_1$ coexist in the region (K_c^b, K_c^f). The above analysis is validated by numerical simulations, as depicted in Fig. 2(a).
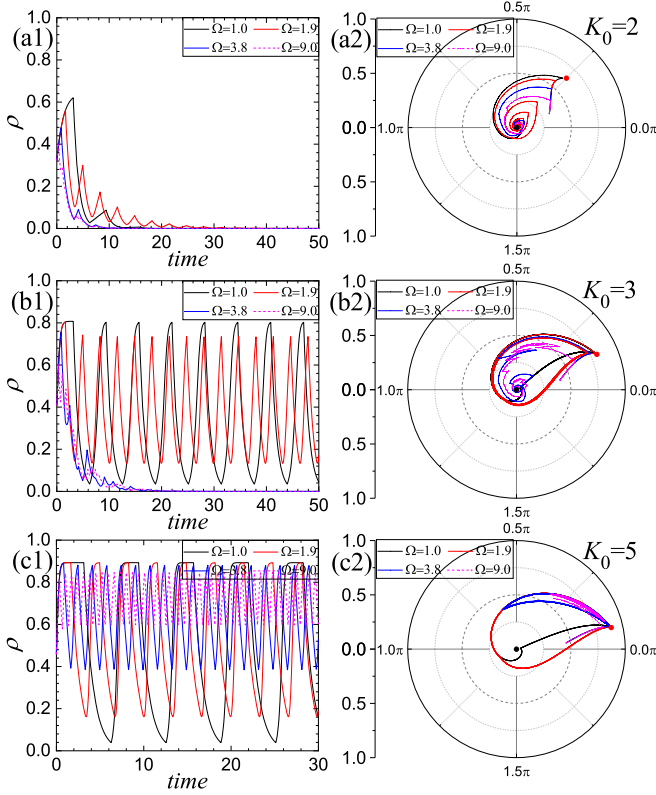
FIG. 3. The synchronization mechanism revealed by the approach of dimension reduction with "on-off" couplings. The left column shows the time evolution of the local synchronization order parameter, ρ, under different driving frequencies, Ω. The right column shows the trajectory of the system dynamics in the polar coordinates. The desynchronization state ($\rho = 0$) and the partial synchronization state ($\mathcal{S}_1$) are marked by the black and red discs, respectively. (a) $K_0 = 2$. (b) $K_0 = 3$. (c) $K_0 = 5$.

Shown in Fig. 2(b) is the variation of the phase difference, ψ, with respect to K_0. We see that the phase difference ψ is locked for $K_0 > K_c^f$ and, as K_0 increases from K_c^f, the value of ψ is gradually decreased, signifying the improved synchronization at large K_0. (Besides the steady states, the order parameter ρ might also oscillate periodically with time under constant couplings, namely the standing-wave state [20]. The standing-wave state is observable in the multistable region (K_c^b, K_c^f) when ω_0 is large enough [40].)

B. The macroscopic mechanism revealed by the reduced model

We move on to analyze the dynamical behavior of the synchronization order parameter, ρ, under the "on-off" couplings. In this scenario, the coupling strength will be alternating between 0 and $2K_0$ periodically and, as a consequence, the order parameter will oscillate with time. Setting $K_0 = 2$, we plot in Fig. 3(a1) the time evolution of ρ under different driving frequencies, $\Omega = (1.0, 1.9, 3.8, 9.0)$. The results are obtained by solving Eq. (12) numerically, with the initial conditions being chosen as $(\rho_1/2, \psi_1/2)$. We see that ρ approaches 0 in all cases. Shown in Fig. 3(a2) is the trajectory of the system dynamics in the polar coordinates, in which the desynchronization state ($\rho = 0$) and the steady state $\mathcal{S}_1$ are marked

as black and red discs, respectively. We see that, though the trajectory is evolving toward $\mathcal{S}_1$ during the "on" episodes, it is the desynchronization state that wins out over the competition eventually. That is, for small values of K_0, the desynchronization state is more stable than the steady state $\mathcal{S}_1$. This result is consistent with the results shown in Fig. 1(a1) (where $R \approx 0$ for $K_0 < 2.6$) and Fig. 1(a2) (where R is staying at 0 despite the change of Ω).

Plotted in Fig. 3(b) are the results for $K_0 = 3$. Interestingly, we see in Fig. 3(b1) that ρ is approaching 0 for the driving frequencies $\Omega = 3.8$ and 9.0, but is oscillating peridically between a large value (~ 0.8) and a small but nonzero value (~ 0.1) for the driving frequencies $\Omega = 1.0$ and $\Omega = 1.9$. Specifically, the time-averaged synchronization order parameter is about $\langle \rho(t) \rangle = 0.45$ for $\Omega = 1.9$ and $\langle \rho(t) \rangle = 0.42$ for $\Omega = 1.0$. The trajectories of the system dynamics are plotted in Fig. 3(b2), where it is seen that the trajectory is swinging between the desynchronization state and the steady state $\mathcal{S}_1$ under the frequencies $\Omega = 1.0$ and 1.9. As the natural frequency of ρ is $2\omega_0 = 2.0$ [as depicted in Eq. (12)], the large-amplitude oscillations of ρ therefore are attributed to the resonance between the driving signals ($\Omega = 1$ and 1.9) and the dynamics of ρ. These results are consistent with the results shown in Fig. 1(a), too, where it is observed that the synchronization performance is significantly affected by the driving frequency Ω only for the intermediate coupling strength (e.g., $K_0 = 3$).

Shown in Fig. 3(c) are the results for $K_0 = 5$. We see in Fig. 3(c1) that ρ is oscillating with time for all the driving frequencies but with different amplitudes. Specifically, with the increase of Ω, the mean value of ρ is increased while the oscillating amplitude is decreased. (The time-averaged synchronization order parameters for $\Omega = 1.0$, 1.9, 3.8, and 9.0 are about 0.4, 0.6, 0.7, and 0.75, respectively.) The trajectories of the system dynamics in the polar coordinates are plotted in Fig. 3(c). We see that when Ω is large (e.g., $\Omega = 9$), the trajectory is oscillating around the steady state $\mathcal{S}_1$ with small amplitudes. However, for the resonant frequencies $\Omega = 1.0$ and 1.9, the trajectory is able to visit the desynchronization state during the "off" episodes, resulting in the decreased synchronization order parameter. This explains the behavior of R for the parameter $K_0 = 8$ plotted in Fig. 1(a2), where it is seen that R reaches the minima around the resonant frequencies.

C. The approach of synchronization transition tree

The approach of dimension reduction reveals only the collective behaviors of the oscillators at the macroscopic level (i.e., the dynamics of the synchronization order parameter), which does not provide information about the microscopic state of the oscillators. For instance, we observe in Fig. 1(a1) that the synchronization order parameter undergoes a crossover in the transition regime (at about $K_0 = 5$) under the resonant frequency $\Omega = 1.9$, yet the underlying mechanism remains not clear. To explore the microscopic state of the oscillators, as well as to deepen our understanding of the influence of periodic coupling on synchronization performance, we finally investigate the synchronization transition by the approach of effective frequencies (transition tree) [11,17].
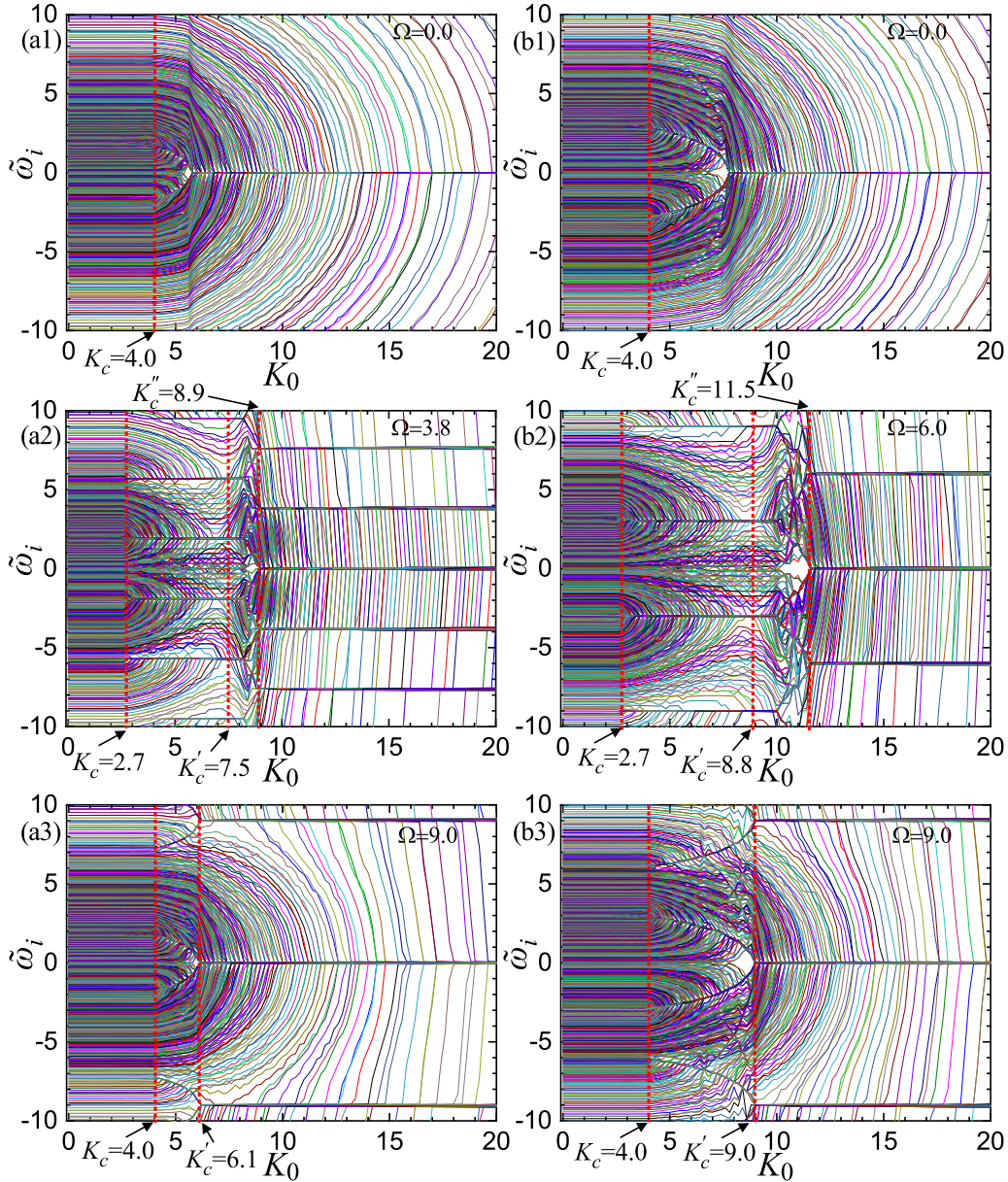
FIG. 4. The impact of coupling frequency on synchronization transition tree. (a)$\omega_0 = 2.0$. (b)$\omega_0 = 3.0$. To better demonstrate the bifurcations, only 2000 oscillators are sampled and the effective frequencies $\tilde{\omega}$ of the oscillators are restricted to be within the range $[-10, 10]$. Dotted vertical lines denote the critical couplings for synchronization. K_c: The critical coupling characterizing the onset of synchronization. K_c': The critical coupling where the clusters are broken. K_c'': The critical coupling whether the oscillators are reorganized into new clusters.

The effective frequencies of the phase oscillators are defined as [11,17]

$$\tilde{\omega}_i = \frac{1}{T} \int_{\tau}^{\tau+T} \dot{\theta}_i(t)dt, \tag{13}$$

where $\dot{\theta}_i(t)$ is the instant frequency of oscillator i, τ is the transient period and T is the time period over which the result is averaged. If oscillators i and j are locked in phase, then we have $\tilde{\omega}_i = \tilde{\omega}_j$, otherwise $\tilde{\omega}_i \neq \tilde{\omega}_j$. In general, the closer effective frequencies between two oscillators, the higher the synchronization degree between them. By tracing the variation of the effective frequencies of all oscillators, we are able to portray the tree-structure bifurcations in the transition from

desynchronization to global synchronization. In simulations, we obtain the transition tree by solving Eq. (1) numerically, while setting $\tau = 200$ and $T = 100$ in calculating the effective frequencies. Fixing $\omega_0 = 2$, we plot in Fig. 4(a) the transition trees generated by different driving frequencies, $\Omega = (0, 3.8, 9.0)$. The results of constant coupling are shown in Fig. 4(a1) for comparison purposes. We see in Fig. 4(a1) that with the increase of K_0, first the effective frequencies around the central frequencies $\pm\omega_0$ become identical (at about $K_c \approx 4.0$), forming two small-size synchronization clusters. Then, as K_0 increases from K_c, the two clusters are gradually combined into a single cluster centered at $\tilde{\omega} = 0$. As K_0 increases further, the cluster is expanding in size by recruiting

more oscillators by the ascending sequence of their natural frequencies.

The results for $\Omega = 3.8$ are plotted in Fig. 4(a2). As $\omega_0 = 2$, we have $\Omega \approx 2\omega_0$ in this case, i.e., the coupling frequency is close to the intrinsic frequency of the local synchronization parameter ρ. Figure 4(a2) shows that two clusters are formed at about $K_c = 2.7$, with the effective frequencies of the clusters being about $\pm\omega_0$. In addition to this, four small-size clusters are also generated at K_c. The central frequencies of these smaller clusters are located at about ± 5.7 and ± 9.5. As K_0 increases from K_c, all six clusters are growing in size. The growth of the clusters, however, is stopped at about $K_c' = 7.5$, where the clusters are broken. As a consequence, the synchronization order parameter is decreased at this point. At about $K_c'' = 8.9$, the oscillators are reorganized into five new clusters, with the central frequencies of the clusters being around 0, ± 3.8 and ± 7.6. After that, as K_0 increases from K_c'' further, the sizes of the new clusters grow gradually, resulting in the increase of the synchronization order parameter. It is just the reorganization of the clusters during the interval $K_0 \in (K_c', K_c'')$ that generates the crossover of the synchronization order parameter in the transition regime [i.e., the crossover at about $K_0 = 8.4$ for the results of $\Omega = 3.8$ shown in Fig. 1(b1)]. As the effective frequencies of the new clusters are resonant with the driving frequency of the periodic coupling, the crossover phenomenon thus lies in the resonance between the synchronization clusters and the periodic coupling.

New features appear in the synchronization transition tree when the driving frequency is large. Shown in Fig. 4(a3) is the transition tree for $\Omega = 9.0$. In this case, two clusters are formed around $\pm\omega_0$ at about $K_c = 4.0$ [which is the same as the case of constant coupling shown in Fig. 4(a1)]. At about $K_c' = 6.1$, the two clusters are merged into a single one whose effective frequency is $\tilde{\omega} = 0$. In addition to this, two small-size clusters are also formed at K_c', with their effective frequencies located at about $\tilde{\omega} = \pm 9.0$. Still, the two small-size clusters are induced by periodic couplings, which happens when K_0 is large enough. After that, as K_0 increases further, the sizes of the three clusters grow gradually, with most oscillators being attracted to the central cluster. As the clusters are not reorganized in this case, the phenomenon of synchronization crossover is absent in the transition regime.

With the synchronization transition trees, we now can interpret the synchronization behaviors observed in direct simulations from a new perspective. In what follows, we take the results of $\Omega = 3.8$ shown in Fig. 1(b) as the example to analyze the influence of periodic coupling on synchronization. First, the enhanced synchronization (showing as the decreased critical coupling for the onset of synchronization) by the periodic coupling ($\Omega = 3.8$) is due to the early formation of the synchronization clusters around the central frequencies $\pm\omega_0$, which is induced by the resonance between the periodic driving and the clusters, as depicted in Fig. 4(a2). Second, the crossover of the synchronization order parameter in the transition regime for the driving frequency $\Omega = 3.8$ is due to the reorganization of the synchronization clusters. Before the reorganization, there are 6 small-size clusters. At the crossover point [$K_0 \approx 8.4$ in Fig. 1(b1)], the clusters are reorganized into 5 large-size clusters whose effective

frequencies are completely different from the former clusters. Third, the suppressing effect of periodic coupling on synchronization under strong couplings ($K_0 > 10$) is rooted again in the resonance between the synchronization clusters and the periodic drivings. For the specific results of $\Omega = 3.8$ shown in Fig. 4(a2), 5 clusters are generated at large K_0; for the results of $\Omega = 9.0$ shown in Fig. 4(a3), 3 clusters are generated. As more synchronization clusters mean less coherent motions, synchronization therefore is suppressed by periodic couplings under strong couplings.

To check the generality of the synchronization scenarios revealed above, we plot in Fig. 4(b) the transition trees for the parameter $\omega_0 = 3$. We see that the synchronization scenarios are essentially the same as that of $\omega_0 = 2$. In specific, Figure 4(b2) shows that under the resonant frequency $\Omega = 6.0$, the oscillators around the effective frequencies $\pm\omega_0$ and $\pm 3\omega_0$ are synchronized into four small-size clusters at $K_c \approx 2.7$. The clusters are growing in size as K_0 increases from K_c to $K_c' \approx 8.8$, and are broken and reorganized into three new clusters at $K_c'' \approx 11.5$. Again, we see that the onset point for synchronization is advanced and the synchronization degree experiences a crossover in the transition regime due to the reorganization of the clusters.

IV. DISCUSSIONS AND CONCLUSIONS

The key to understanding the impact of periodic coupling on synchronization lies in the way how the oscillators are organized into clusters. As depicted in Fig. 4, a distinctive feature of the synchronization transition trees under the resonant frequencies is the reorganization of the clusters in the transition to global synchronization. Taking the results shown in Fig. 4(a2) as an example, we see in this figure that as K_0 increases from $K_c \approx 2.7$, 6 small-size synchronization clusters are generated first, with the effective frequencies of the clusters being around $\pm\omega_0$, $\pm 3\omega_0$ and $\pm 5\omega_0$. As K_0 increases from K_c to $K_c' \approx 7.5$, the clusters are growing in size but the effective frequencies of the clusters are kept unchanged. The clusters, however, are broken and reorganized into five new clusters as K_0 increases from K_c' to $K_c'' \approx 8.9$. The effective frequencies of the new clusters are at about 0, $\pm\Omega$ and $\pm 2\Omega$. Compared to the results of the nonresonant frequencies [e.g., the Figs. 4(a1) and 4(a3)], the impact of the resonant coupling thus is featured by the range $K_0 \in (K_c, K_c')$: the smaller the value of K_c, the earlier the onset of synchronization; the larger the value of K_c', the later the crossover of the synchronization order parameter appeared in the synchronization transition. To have a global picture on the dependence of this resonant range on the driving frequency, we plot in Fig. 5 the heat map of the synchronization order parameter in the two-dimensional parameter space (Ω, K_0). The results are obtained by direct simulations of Eq. (1), which involves massive computing resources. Three cases of frequency distribution have been considered in our simulations, $\omega_0 = (1.0, 2.0, 3.0)$. We see that (1) the critical coupling K_c is markedly decreased around the resonant frequency $\Omega = 2\omega_0$ (the red, vertical dotted lines) and (2) a resonant tongue appears in the variation of the critical coupling K_c' (the black, dotted curves). We also see that by increasing the coupling amplitude K_0, the resonant tongue
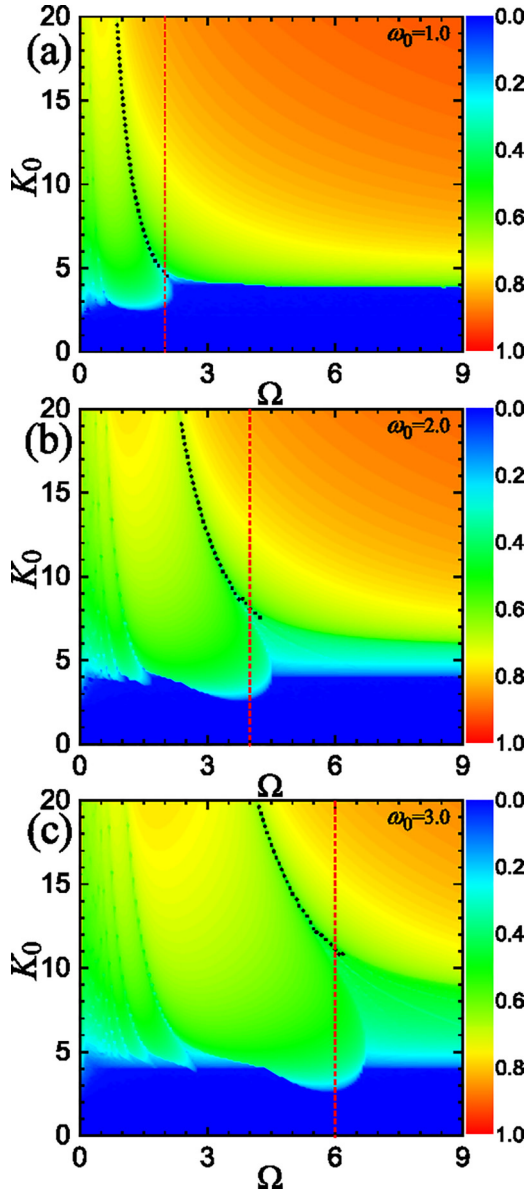
FIG. 5. Heat maps of the synchronization order parameter, R, on the parameter space (Ω, K_0). (a)$\omega_0 = 1.0$. (b)$\omega_0 = 2.0$. (a)$\omega_0 = 3.0$. Vertical dotted lines denote the resonant frequency $\Omega = 2\omega_0$. Dotted curves denote the critical coupling, K'_c, characterizing the crossover point in the synchronization transition.

is shifted leftward slightly, indicating that the crossover point is delayed as Ω deviates from the resonant frequency.

Our studies extend the current knowledge on the synchronization behaviors of coupled phase oscillators in two aspects. First, our studies show that the adoption of periodic coupling can improve the synchronization performance of coupled phase oscillators. Two conditions are identified as necessary for improving the synchronization performance: (1) the natural frequency of the oscillators should follow a bimodal distribution and (2) the driving frequency of the periodic coupling should be close to the distance of the central frequencies in the distribution. The improving effect of periodic coupling on synchronization is reflected in the decreased critical coupling for the onset of synchronization, which is

rooted in the resonance between the periodic coupling and the synchronization clusters formed by oscillators whose natural frequencies are around the central frequencies. This finding is in contrast to the results obtained in coupled phase oscillators with unimodal frequency distributions, where it is shown that the adoption of periodic coupling always suppresses synchronization [37]. Second, our studies demonstrate that in the transition to the global synchronization state, the synchronization order parameter of the system undergoes a crossover at some critical coupling. In exploring the synchronization transition of Kuramoto-like models, a common observation is that after the onset of synchronization, the synchronization order parameter is increased monotonically with the increase of the coupling strength [8–12]. Our studies based on synchronization transition trees reveal that the crossover of the synchronization order parameter is due to the reorganization of the synchronization clusters. Before the crossover point, the synchronization clusters are organized mainly around the central frequencies of the bimodal distribution, while after that the clusters are organized around the harmonic frequencies of the periodic coupling. It is just the competition between the two clustering mechanisms that lead to the crossover phenomenon.

As the final remark, we note that depending on the system parameters $(\omega_0, \Delta, K_0, \Omega)$, the reduced model as described by Eq. (12) can present a variety of dynamics, including steady states, periodic states, and chaotic states [20,41]. In particular, when the amplitude of the periodic coupling, K_0, is moderate, the behavior of the order parameter, ρ, could be chaotic. The chaotic states are sparse in the parameter space (Ω, K_0) and are mainly distributed in the resonant regions. The emergence of chaos might be attributed to the competition of the synchronization clusters in the process of cluster reorganization [40].

To summarize, inspired by the facts that the natural frequencies of the dynamical units in complex systems might not follow the unimodal distribution and the coupling strength between the units might change with time, we have investigated the synchronization behaviors of globally coupled phase oscillators, with the natural frequencies of the oscillators following the bimodal Lorentzian frequency and the coupling strength is changing with time periodically. It is found that the synchronization performance of the oscillators can be significantly affected by adopting periodic couplings. Specifically, for weak couplings, the critical coupling for the onset of synchronization can be markedly decreased by a proper setting of the coupling frequency; for strong couplings, the synchronization order parameter undergoes a crossover in the transition to global synchronization. The mechanisms underlying the observed phenomena have been investigated by the approaches of dimension reduction and synchronization transition tree. It is revealed that the advanced synchronization onset is induced by the resonance between the periodic coupling and the synchronization clusters, and the crossover of the synchronization order parameter is due to the reorganization of the synchronization clusters in the transition to global synchronization. Our studies give a glimpse into the rich dynamics induced by the resonance between synchronization clusters and periodic coupling in coupled phase oscillators, and many intriguing phenomena (questions) remain to be explored (addressed) in the future, e.g, the adoptions of multimodal frequency

distributions, the cases of complex networks, and the situations of quasiperiodic or stochastic couplings. We hope the present work could be the starting point for a new direction in exploring the synchronization behaviors in Kuramoto-like models.

APPENDIX: SYMMETRY OF CLUSTER-BASED SYNCHRONIZATION ORDER PARAMETERS IN THE REDUCED MODEL

In obtaining the reduced model [see Eq. (12)] from Eq. (11), we have assumed that the synchronization order parameters of the two clusters are identical, i.e., $\rho_1(t) = \rho_2(t) = \rho(t)$. We now justify this assumption by providing mathematical proof (the numerical evidence is given in the Supplemental Material [40]). As the local stability of this symmetric solution has been analyzed in Ref. [20], here we focus on only the uniqueness of this solution. That is, we are going to prove that the symmetric solution $\rho_1(t) = \rho_2(t)$ is the unique solution of Eq. (11).

We analyze first the symmetry of the synchronization order parameters for the incoherent states observed in the range $K_0 \in [0, K_c)$. As $R = \sqrt{\rho_1^2 + \rho_2^2 + 2\rho_1\rho_2 \cos\psi} = 0$ and ψ is time-dependent, we have $\rho_1 = \rho_2 = 0$ in this case, which satisfies the symmetric condition.

We next analyze the symmetry of the synchronization order parameters for the partially coherent states generated for

$K_0 > K_c$. Setting $z_{1,2} = \rho_{1,2}e^{\mathbf{i}\phi_{1,2}}$ in Eq. (11), we have

$$\dot{\rho}_1 = -\Delta\rho_1 + K(t)(1 - \rho_1^2)(\rho_1 + \rho_2 \cos\psi)/4,$$

$$\dot{\rho}_2 = -\Delta\rho_2 + K(t)(1 - \rho_2^2)(\rho_2 + \rho_1 \cos\psi)/4,$$

$$\dot{\psi} = 2\omega_0 - K(t)(\rho_1^2 + \rho_2^2 + 2\rho_1^2\rho_2^2)\sin\psi/(4\rho_1\rho_2), \quad \text{(A1)}$$

with $\psi = \phi_2 - \phi_1$ the phase difference between the synchronization order parameters of the clusters. The general solution of Eq. (A1) is $\rho_2(t) = \alpha(t)\rho_1(t)$, with $\alpha(t)$ positively defined. Inserting this solution into Eq. (A1) (only for the equations of ρ_1 and ρ_2) and after some algebra, we have

$$\dot{\alpha}(t) + \frac{K(t)}{4}[\alpha^2(t) - 1](\cos\psi + \rho_1\rho_2) = 0. \quad \text{(A2)}$$

One solution of Eq. (A2) is $\alpha(t) = 1$, i.e., $\rho_1(t) = \rho_2(t)$. Assume that Eq. (A2) has other solution with $\alpha(t) \neq 1$, the integration of Eq. (A2) gives

$$\ln\left|\frac{1 + \alpha(t)}{1 - \alpha(t)}\right| = \int \frac{K(t)}{2}(\cos\psi + \rho_1\rho_2)dt. \quad \text{(A3)}$$

We see that if $\alpha(t) = \rho_2(t)/\rho_1(t)$ is a solution of Eq. (A3), then $1/\alpha(t) = \rho_1(t)/\rho_2(t)$ must be also a solution of the equation. Inserting the new solution $1/\alpha(t)$ into Eq. (A2), we have the equation

$$K(t)(\cos\psi + \rho_1\rho_2)\left[\frac{1}{\alpha^2(t)} - \alpha^2(t)\right] = 0,$$

which has only one solution, $\alpha(t) = 1$ (please note that $\alpha(t)$ is positively defined). As this solution is obtained with the assumption $\alpha(t) \neq 1$, the contradiction therefore leads to the conclusion that the symmetric solution with $\alpha(t) = 1$ is the only solution of Eq. (A1). This completes the proof.

Numerical simulations have been conducted to check the uniqueness and stability of the symmetric solution, which confirm that the symmetric solution is unique and globally attractive for the dynamics described by Eq. (11) [40].

[1] Y. Kuramoto, *Chemical Oscillations, Waves, and Turbulence* (Springer, Berlin, 1984).

[2] J. A. Acebrón, L. L. Bonilla, C. J. Pérez Vicente, F. Ritort, and R. Spigler, The Kuramoto model: A simple paradigm for synchronization phenomena, Rev. Mod. Phys. **77**, 137 (2005).

[3] F. A. Rodrigues, T. K. D. Peron, P. Ji, and J. Kurths, The Kuramoto model in complex networks, Phys. Rep. **610**, 1 (2016).

[4] Y. Kuramoto, Self-entrainment of a population of coupled nonlinear oscillators, in *International Symposium on Mathematical Problems in Theoretical Physics*, edited by H. Araki, Lecture Notes in Physics (Springer, Berlin, 1975), Vol. 39, pp. 420–422.

[5] S. H. Strogatz, From Kuramoto to Crawford: Exploring the onset of synchronization in populations of coupled oscillators, Physica D **143**, 1 (2000).

[6] A. Arenas, A. Díaz-Guilera, J. Kurths, Y. Moreno, and C. S. Zhou, Synchronization in complex networks, Phys. Rep. **469**, 93 (2008).

[7] Y. Moreno and A. F. Pacheco, Synchronization of Kuramoto oscillators in scale-free networks, Europhys. Lett. **68**, 603 (2004).

[8] D.-S. Lee, Synchronization transition in scale-free networks: Clusters of synchrony, Phys. Rev. E **72**, 026208 (2005).

[9] J. Gómez-Gardeñes, Y. Moreno, and A. Arenas, Paths to synchronization on complex networks, Phys. Rev. Lett. **98**, 034101 (2007).

[10] S. G. Guan, X. G. Wang, Y.-C. Lai, and C.-H. Lai, Transition to global synchronization in clustered networks, Phys. Rev. E **77**, 046211 (2008).

[11] J. Gómez-Gardeñes, S. Gómez, A. Arenas, and Y. Moreno, Explosive synchronization transitions in scale-free networks, Phys. Rev. Lett. **106**, 128701 (2011).

[12] R. Berner, S. Vock, E. Schöll, and S. Yanchuk, Desynchronization transitions in adaptive networks, Phys. Rev. Lett. **126**, 028301 (2021).

[13] Y. Kuramoto and D. Battogtokh, Coexistence of coherence and incoherence in nonlocally coupled phase oscillators, Nonlin. Phenom. Complex Syst. **5**, 380 (2002).

[14] D. M. Abrams, R. Mirollo, S. H. Strogatz, and D. A. Wiley, Solvable model for chimera states of coupled oscillators, Phys. Rev. Lett. **101**, 084103 (2008).

[15] X. Li, T. Qiu, S. Boccaletti, I. Sendiña-Nadal, Z. H. Liu, and S. G. Guan, Synchronization clusters emerge as the result of a global coupling among classical phase oscillators, New J. Phys. **21**, 053002 (2019).

[16] M. Kato and H. Kori, Partial synchronization and community switching in phase-oscillator networks and its analysis based on a bidirectional, weighted chain of three oscillators, Phys. Rev. E **107**, 014210 (2023).

[17] Z. Zheng, G. Hu, and B. Hu, Phase slips and phase synchronization of coupled oscillators, Phys. Rev. Lett. **81**, 5318 (1998).

[18] E. Montbrió, D. Pazó, and J. Schmidt, Time delay in the Kuramoto model with bimodal frequency distribution, Phys. Rev. E **74**, 056201 (2006).

[19] D. Pazó and E. Montbrió, Existence of hysteresis in the Kuramoto model with bimodal frequency distributions, Phys. Rev. E **80**, 046215 (2009).

[20] E. A. Martens, E. Barreto, S. H. Strogatz, E. Ott, P. So, and T. M. Antonsen, Exact results for the Kuramoto model with a bimodal frequency distribution, Phys. Rev. E **79**, 026204 (2009).

[21] H. J. Bi, X. Hu, S. Boccaletti, X. G. Wang, Y. Zou, Z. H. Liu, and S. G. Guan, Coexistence of quantized, time dependent, clusters in globally coupled oscillators, Phys. Rev. Lett. **117**, 204101 (2016).

[22] J. M. Zhang, S. Boccaletti, Z. H. Liu, and S. G. Guan, Synchronization of phase oscillators under asymmetric and bimodal distributions of natural frequencies, Chaos Solitons Fractals **136**, 109777 (2020).

[23] M. Manoranjani, R. Gopal, D. V. Senthilkumar, V. K. Chandrasekar, and M. Lakshmanan, Influence of asymmetric parameters in higher-order coupling with bimodal frequency distribution, Phys. Rev. E **105**, 034307 (2022).

[24] M. Edwards and A. J. Richardson, Impact of climate change on marine pelagic phenology and trophic mismatch, Nature (London) **430**, 881 (2004).

[25] S. M. Reppert and D. R. Weaver, Coordination of circadian timing in mammals, Nature (London) **418**, 935 (2002).

[26] J. Stöckel, E. A. Welsh, M. Liberton, R. Kunnvakkam, R. Aurora, and H. B. Pakrasi, Global transcriptomic analysis of *Cyanothece* 51142 reveals robust diurnal oscillation of central metabolic processes, Proc. Natl. Acad. Sci. USA **105**, 6156 (2008).

[27] H. Thomson, Wave therapy, Nature (London) **555**, 20 (2018).

[28] D. Fox, Brain buzz, Nature (London) **472**, 156 (2011).

[29] H. F. Iaccarino, A. C. Singer, A. J. Martorell *et al.*, Gamma frequency entrainment attenuates amyloid load and modifies microglia, Nature (London) **540**, 230 (2016).

[30] H. Sakaguchi, Cooperative phenomena in coupled oscillator systems under external fields, Prog. Theor. Phys. **79**, 39 (1988).

[31] T. M. Antonsen, Jr., R. T. Faghih, M. Girvan, E. Ott, and J. Platig, External periodic driving of large systems of globally coupled phase oscillators, Chaos **18**, 037112 (2008).

[32] L. M. Childs and S. H. Strogatz, Stability diagram for the forced Kuramoto model, Chaos **18**, 043128 (2008).

[33] W. C. Yang, W. J. Lin, X. G. Wang, and L. Huang, Synchronization of networked chaotic oscillators under external periodic driving, Phys. Rev. E **91**, 032912 (2015).

[34] L. Chen, C. Qiu, and H. B. Huang, Synchronization with on-off coupling: Role of time scales in network dynamics, Phys. Rev. E **79**, 045101(R) (2009).

[35] S. S. Li, N. Sun, L. Chen, and X. G. Wang, Network synchronization with periodic coupling, Phys. Rev. E **98**, 012304 (2018).

[36] Z. Dayani, F. Parastesh, F. Nazarimehr, K. Rajagopal, S. Jafari, E. Schöll, and J. Kurths, Optimal time-varying coupling function can enhance synchronization in complex networks, Chaos **33**, 033139 (2023).

[37] S. S. Li, X. G. Wang, and S. G. Guan, Periodic coupling suppresses synchronization in coupled phase oscillators, New J. Phys. **20**, 113013 (2018).

[38] B. Pietras and A. Daffertshofer, Network dynamics of coupled oscillators and phase reduction techniques, Phys. Rep. **819**, 1 (2019).

[39] E. Ott and T. M. Antonsen, Low dimensional behavior of large systems of globally coupled oscillators, Chaos **18**, 037113 (2008).

[40] See Supplemental Material at http://link.aps.org/supplemental/10.1103/PhysRevE.110.024219 for the numerical evidence showing the symmetry of the cluster-based synchronization order parameter, the complicated dynamics of the reduced model, and the synchronization performance under "on-off" couplings.

[41] P. So and E. Barreto, Generating macroscopic chaos in a network of globally coupled phase oscillators, Chaos **21**, 033127 (2011).